Structural and functional characterization of the VirB5 protein from the type IV secretion system encoded by the conjugative plasmid pKM101

Hye-Jeong Yeo*†, Qing Yuan‡, Moriah R. Beck†, Christian Baron‡, and Gabriel Waksman*†§¶

*Institute of Structural Molecular Biology, Birkbeck College, Malet Street, London WC1E 7HX, United Kingdom; §Institute of Structural Molecular Biology, Department of Biochemistry and Molecular Biology, University College London, Gower Street, London WC1E 6BT, United Kingdom; ‡Department of Biology, McMaster University, 1280 Main Street West, Hamilton, ON, Canada LS8 4K1; and †Department of Biochemistry and Molecular Biophysics, Washington University School of Medicine, 660 South Euclid Avenue, St. Louis, MO 63110

Edited by Patricia C. Zambryski, University of California, Berkeley, CA, and approved October 27, 2003 (received for review August 14, 2003)

Type IV secretion systems mediate intercellular transfer of macromolecules via a mechanism ancestrally related to that of bacterial conjugation machineries. TraC of the IncN plasmid pKM101 belongs to the VirB5 family of proteins, an essential component of most type IV secretion systems. Here, we present the structure of TraC. VirB5/TraC is a single domain protein, which consists of a three helix bundle and a loose globular appendage. Structure-based site-directed mutagenesis followed by functional studies indicates that VirB5 proteins participate in protein–protein interactions important for pilus assembly and function.

conjugation | crystal structure | pilus | TraC

Bacterial conjugation systems are macromolecular DNA transfer systems. Their impact on human health is highly significant as conjugation is the major vector for the dissemination of antibiotic resistance genes (1). Recent work has shown that several plant and human pathogens have evolved secretion machineries ancestrally related to conjugation systems for the purpose of delivering virulence effectors (proteins or protein–DNA complexes) to eukaryotic cell targets. Such pathogens include extracellular organisms such as *Agrobacterium tumefaciens*, the causative agent of crown gall disease, *Bordetella pertussis*, the agent responsible for whooping cough in children, and *Helicobacter pylori*, responsible for gastric ulcers and stomach cancer (reviewed in refs. 2–4). More recently, intracellular bacterial pathogens, such as *Brucella suis*, the causative agent for brucellosis, and *Legionella pneumophila*, the causative agent of legionnaire's disease, were shown to require such systems for their virulence (5, 6). Bacterial conjugation systems and their related counterparts in pathogenic bacteria are collectively known as type IV secretion systems (T4SS).

T4SSs form supramolecular assemblies generally composed of a pilus assembly machinery/secretion apparatus that presumably produces a channel for translocation of the effectors. T4SSs consist of ≈8–15 proteins, 12 of which (named VirB1–VirB11 and VirD4 according to the nomenclature of the model T4SS from *A. tumefaciens*) are required for secretion (3, 4). However, very little is known about how these proteins assemble to form the translocation apparatus, and about the functions of each component within the machinery. VirB2 is the major component of the *A. tumefaciens* pilus, and it was shown to undergo cyclization before its incorporation into extracellular pili (7, 8). VirB5 and VirB7 are also associated with the pilus but appear to be minor components (9, 10). The core channel structure is likely formed by VirB7–VirB10 (11–14). Three putative NTPases, VirB4, VirB11, and VirD4, power the secretion apparatus, and VirB4 and VirB11 are also essential for pilus biogenesis (15–18).

Recently, the structures of a VirB11 ATPase ortholog from *H. pylori*, HP0525 (19, 20), and of a VirD4 ATPase ortholog from the conjugative plasmid R388, TrwB, have been determined (21). Both ATPases are hexameric assemblies. TrwB is architecturally related to hexameric helicases, consistent with its role as a coupling factor that links the DNA-processing nucleoprotein complex, the relaxosome, with the transport apparatus during mating (22). VirB11 has a very different architecture and is related to proteins such as p97 and *N*-ethylmaleimide *s*ensitive *f*actor (NSF) involved in assembly and disassembly of the vesicle fusion apparatus in eukaryotes (20), suggesting that VirB11 may be involved in similar functions in T4SSs.

Here, we present a structure of a VirB5 protein, TraC, the VirB5 homolog encoded by the pKM101 plasmid, and describe a biological characterization of site-directed TraC/VirB5 variants mutated in important regions of the structure. VirB5 has been shown to be a minor component of the pilus in both the *A. tumefaciens* (10) and pKM101 plasmid T4SSs (23). In *Agrobacterium*, VirB5 cofractionates with extracellular VirB2, the major pilus component, and also with VirB7, an outer-membrane protein (9, 24). Sequences of ≈15 VirB5 proteins are currently available in the Protein Data Bank (PDB). These proteins are characteristically ≈220 residues in length and acidic (theoretical pI 4–5), and contain N-terminal signal peptide sequences targeting the protein to the periplasmic space. Despite the fact that VirB5 proteins are essential for type IV secretion (except in *B. pertussis*, where VirB5 is absent), little is known about the functions that these proteins fulfill in these machineries.

Methods

Overproduction and Purification of Selenomethionyl TraC (SeMetTraC) Protein from *Escherichia coli* Plasmid pKM101. A pVS1-based broad host range plasmid containing the strong P_{trc} promoter (pTrcTraC) was used for overproduction of the protein in *E. coli* JM109 (23). For SeMetTraC protein production, the metA$^-$ strain DL41 was used. The protein was extracted from the periplasm, precipitated in 45% ammonium sulfate, and further purified by a three-step purification procedure that includes anion-exchange chromatography, hydrophobic interaction chromatography, and size exclusion chromatography (see supporting information, which is published on the PNAS web site).

Crystallization and Data Collection. Crystals of SeMetTraC were grown at room temperature by vapor diffusion in hanging drops against a reservoir solution containing 1.26–1.34 M $(NH_4)_2SO_4$, 100 mM Na-Citrate (pH 6.25), 0.2 M NaCl, and 5% glycerol. Crystals were in rhombohedral space group R32 with cell dimension $a = b = 144.7$ Å and $c = 92.28$ Å. Three SAD data sets

This paper was submitted directly (Track II) to the PNAS office.

Abbreviations: T4SS, type IV secretion system; SeMet, selenomethionine.

Data deposition: The atomic coordinates and structure factors have been deposited in the Protein Data Bank, www.rcsb.org (PDB ID code 1R8I).

¶To whom correspondence should be addressed. E-mail: g.waksman@mail.cryst.bbk.ac.uk.

Table 1. Data collection and refinement statistics

Data collection	
λ, Å	
SeMet-1	0.97931
SeMet-2	0.97931
SeMet-3	0.97931
Resolution, Å	
SeMet-1	3.1
SeMet-2	3.0
SeMet-3	3.0
Reflections, total/unique	
SeMet-1	95,810/12,305
SeMet-2	103,125/13,197
SeMet-3	106,523/13,072
Completeness, (%)	
SeMet-1	95.2 (98.2)
SeMet-2	98.5 (92.8)
SeMet-3	92.1 (92.1)
R_{sym} (%)*	
SeMet-1	7.8 (37.5)
SeMet-2	7 (32.4)
SeMet-3	6.8 (30.1)
I/σ (I)	
SeMet-1	20.9 (7.2)
SeMet-2	19.2 (2.7)
SeMet-3	21.4 (3.2)
Refinement	
Resolution, Å	25–3.0
$\|F\|/\sigma$ ($\|F\|$)	>0
No. reflections, working/test	11,628/1,381
Total no. of atoms	1,370
R/R_{free}†	26.36/28.83
rms deviation	
Bonds, Å	0.009
Angles, °	1.38
B values (main chain/side chain), Å^2	1.3/2.1

Numbers in parentheses correspond to values in the highest resolution shell [3.21–3.10 (SeMet-1), 3.11–3.0 (Semet-2 and SeMet-3)].

*$R_{sym} = \Sigma|I - \langle I\rangle|\Sigma I$, where I is observed intensity and $\langle I\rangle$ is the average intensity for symmetry-related functions.

†$R = \Sigma|F_o - F_c|\Sigma F_o$, R_{free} is calculated for test set reflections (10%) randomly excluded from refinement.

at the selenium absorption peak were collected [selenomethionines (SeMets)-1 to -3 in Table 1]. Data were processed with DENZO and SCALEPACK (25).

Structure Determination and Refinement. Crystals contain one molecule per asymmetric unit. TraC contains 13 SeMets. When the program SOLVE (26) and the SeMet-1 data collected at the absorption peak were used, the position of eight Se sites could be found reliably. Three additional peaks were found by using the SeMet-3 data, and a 12th site was detected by the program ADD SOLVE using the SeMet-2 data set and phases calculated from the four highest Se peaks. The 12 identified sites were then used in phasing by using the SAD phasing method followed by density modification (solvent flipping) as implemented by the program CNS (27). The electron density map was further improved by combination of the phase sets obtained with each of the three data sets. The resulting 3.0-Å electron density map was readily interpretable (Fig. 1*A*), and a model was built by using the program O (28, 29). The resulting atomic model was refined by using conjugate gradient minimization (program CNS). An overall anisotropic temperature factor was applied throughout the refinement. The final model includes 1,370 atoms of residues 32–218 in the asymmetric unit (see Table 1 for refinement statistics). The model has been deposited in the PDB (entry code 1R8I).

Cloning of TraC Mutants. Mutations of residues were introduced to the plasmid pTrcTraC containing the full-length *traC* gene by standard PCR methods (QuikChange kit from Stratagene) and confirmed by sequencing (see supporting information). Phage infection experiments required low-level expression of *traC*; to this end, an AraC–pBAD expression cassette was introduced into the backbone of the pVS1-based expression system by using standard methods. TraC and TraC variants were cloned downstream of this cassette to yield pVSBADTraC and variants (see supporting information). TraC variants were expressed and purified as wild type.

Biological Assays of TraC Functions. Fractionation of surface-exposed pili, detection of TraC and its mutated derivatives in cell lysates and extracellular high molecular mass structures, and complementation of conjugative transfer were performed as described in ref. 23. To determine the ability of different TraC derivatives to restore the phage sensitivity of FM433 pKM101*traC*, the cells were transformed with pVSBADTraC constructs expressing the wild-type or different mutant genes. Growth of phages PRD1 and IKe were monitored as described in ref. 30.

Sedimentation Equilibrium of TraC and TraC Mutants. Sedimentation experiments were conducted in a Beckman XL-A Optima analytical ultracentrifuge equipped with absorbance optics and an An60Ti rotor. Purified TraC was in a buffer containing 50 mM Tris, 50 mM NaCl, 0.5 mM DTT, and 5% glycerol (pH 8.0). The partial specific volume and solvent density were calculated by using SEDNTERP ($\nu_{TraC} = 0.7305$; $\rho = 0.99846$) (31). Sedimentation equilibrium studies were carried out at 20,000, 24,000, and 28,000 rpm at 20°C. Six-channel, charcoal-filled epon centerpieces with quartz windows were filled with 120 μl of sample at concentrations between 10.2 and 82.6 μM. Absorbance profiles were acquired at 280 nm between 5.9 and 7.3 cm as the average of five measurements, with a step size of 0.001 cm. The raw data files were edited by using the REEDIT program to extract the three channels of data and then analyzed with NONLIN (32).

Results

Overall Structure of TraC. To obtain the three-dimensional structure of a VirB5 protein, we overproduced and purified three members of the VirB5 protein family: pKM101 TraC, *A. tumefaciens* VirB5, and *Brucella suis* VirB5. Only TraC produced crystals. Crystals of TraC diffracted to moderate resolution (3.0 Å) and were sensitive to radiation. Thus, the structure was solved by using the SAD phasing method (Fig. 1*A* and Table 1).

The structure of TraC is presented in Fig. 1*B*. It is a mostly α-helical, elongated, structure. Three long α-helices (α1, α2, and α3) form the backbone of the structure. This backbone supports an α-helical, loose, appendage formed by four short helices, αa, αb, αc, and αd (Fig. 1 *B* and *C*). A 3_{10} helix is present between α1 and αa. Although the core α-helical bundle is very well defined in the electron density, the appendage is characterized by higher temperature factors, suggesting flexibility and mild disorder in that region of the structure.

A structure-based alignment of TraC with other VirB5 proteins is shown in Fig. 1*C* (see also supporting information). Most of the conserved residues between TraC of pKM101, VirB5 from *Brucella suis*, TrwJ of the IncW plasmid R388, and AvhB5 of the *A. tumefaciens* plasmid pAtC58 locate to the hydrophobic core of the protein, suggesting structural similarities. When the program 3D-PROFILE (33) and the structure of TraC are used as a template, the various sequences of VirB5 homologs (including that of *A. tumefaciens* C58 VirB5, which is the least conserved

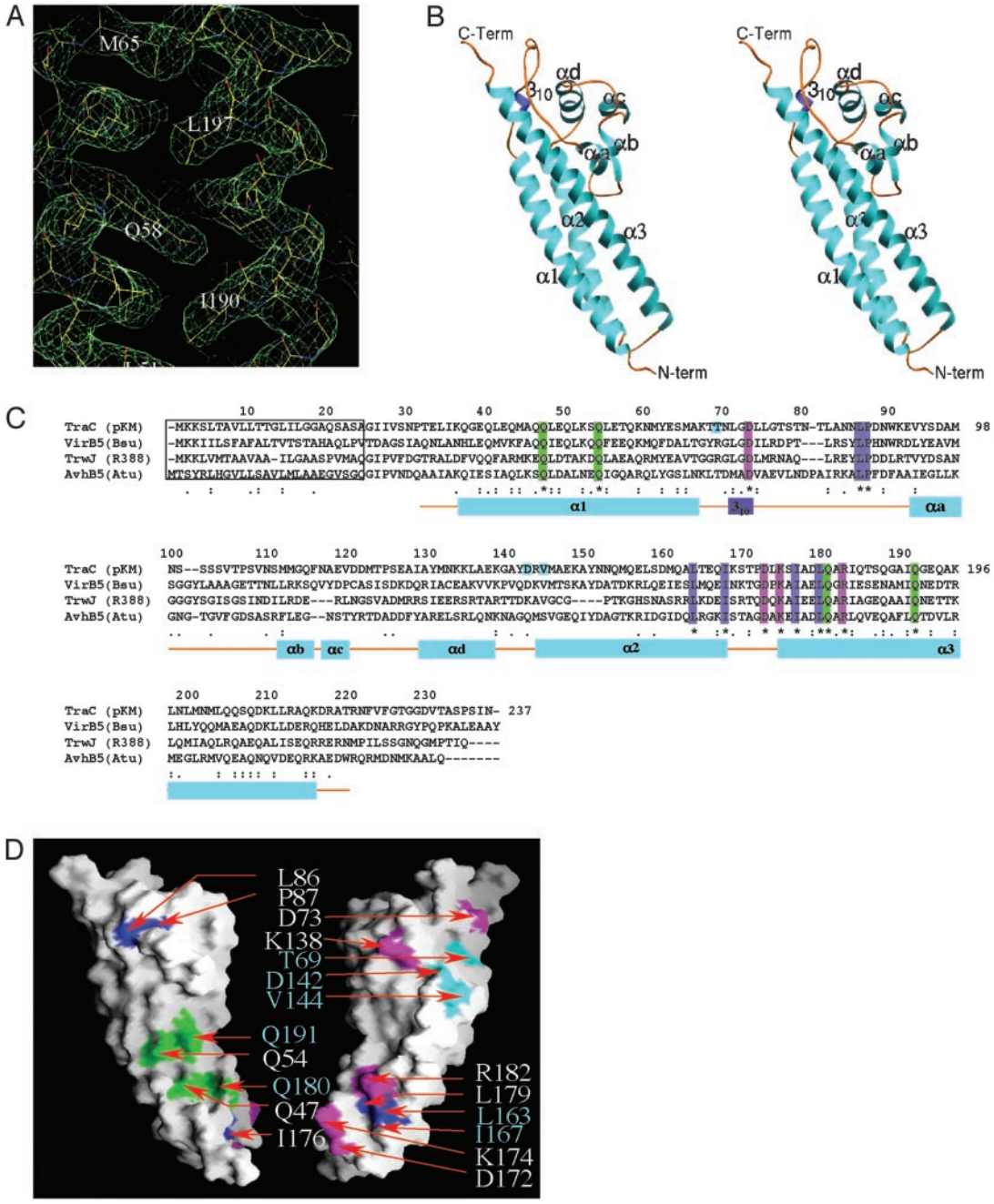

Fig. 1. Crystal structure of TraC. (*A*) Representative electron density at 3-Å resolution. The experimental map was calculated by using SAD phases after solvent flipping and is contoured at a 1.2σ level. The final refined model is shown in stick representation color-coded in yellow for carbon, blue for nitrogen, and red for oxygen. (*B*) Stereo ribbon diagram of the structure of TraC monomer (43). α-helices, 3_{10} helix, and loops are indicated in cyan, blue, and amber, respectively. The three major helices are labeled from α1 to α3, and the short helices between α1 and α2 are labeled from αa to αd. (*C*) Sequence alignment of VirB5 proteins and secondary structure assignment in TraC. Amino acid sequences of four representative VirB5 proteins were aligned, from IncN plasmid pKM101 (TraC pKM), *Brucella suis* (VirB5 Bsu), the IncW plasmid R388 (TrwJ R388), and *A. tumefaciens* plasmid pAtC58 (AvhB5 Atu). Strictly conserved, strongly conserved, and conserved residues are indicated by a star, double dot, or dot symbol, respectively. Amino acid numbering at the top refers to TraC. Secondary structural elements of TraC are shown below the sequences in cyan for α-helices and blue for 3_{10} helices. Strictly conserved residues located at the surface of the protein are indicated by filled boxes, green for Gln residues, magenta for charged residues, and deep blue for hydrophobic residues. Residues located at the putative crystallographic dimer interface and mutated in this study are indicated in cyan boxes. The N-terminal signal peptide sequences are indicated in the black box. (*D*) Conserved solvent-exposed residues at the surface of TraC. Residues located at the putative crystallographic dimer interface are also indicated. Color-coding for residues are as in *C*. The orientation in *Left* is the same as in *B*, whereas in *Right*, the structure has been rotated 180° along the vertical axis. All colored surface residues are labeled. Labels in cyan indicate residues that were mutated.

member of the VirB5 family of proteins; see supporting information) return a high score, indicating that, indeed, the structure of TraC can be considered a prototype for most VirB5 proteins. Close inspection of the sequence alignment presented in Fig. 1*C* also reveals strictly conserved residues, which map to the surface of the protein. Their locations are shown in Fig. 1*D*. A number of charged residues form patches of conserved regions on the surface of the protein (Fig. 1*D Right*, surface residues in ma-

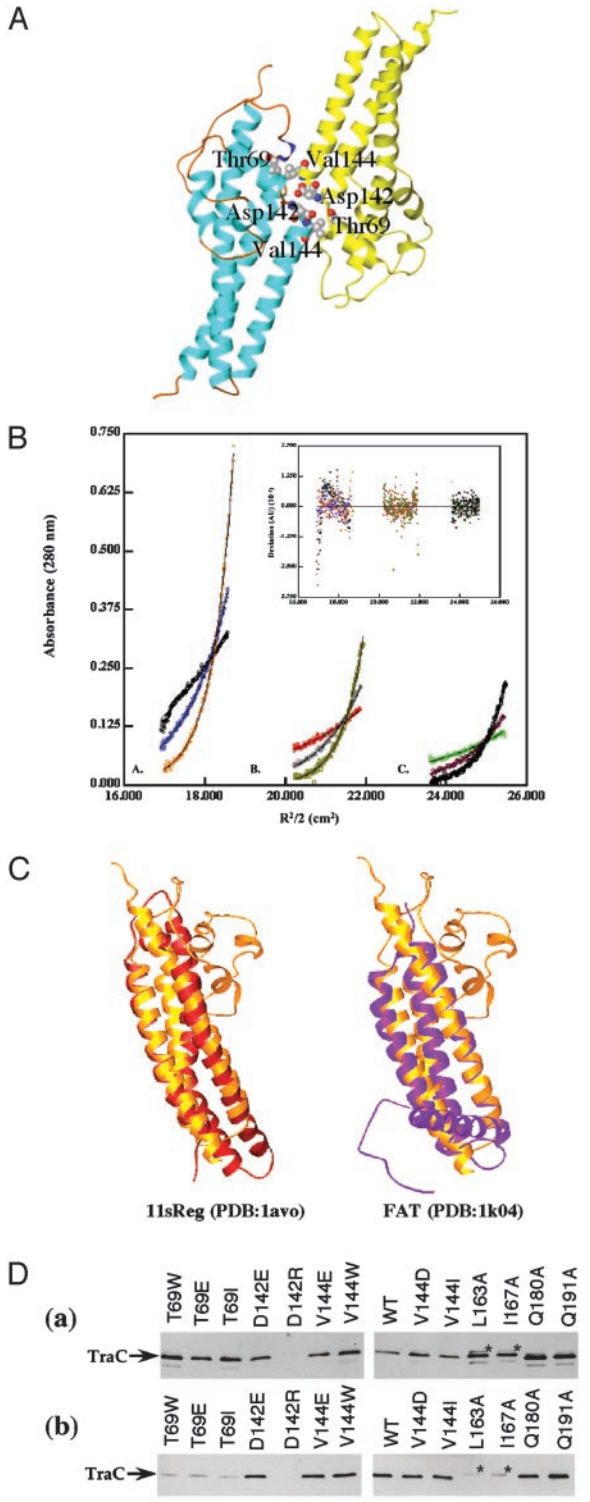

Fig. 2. (*A*) Putative crystallographic dimer interface and location of Thr-69, Asp-142, and Val-144. Each subunit in the dimer is in ribbon representation. Indicated residues are in space-filling representation. (*B*) Sedimentation equilibrium of TraC. The circles are the measured values in the standard three sample sectors (A–C) of the ultracentrifugation cell for experiments conducted at three speeds (which differ by color). Loading concentrations, in total monomer, are as follows: A, 0.97; B, 0.48; and C, 0.24 mg/ml. The solid line is the result of fitting the data to a single-ideal species model by using the regression analysis NONLIN program. The residuals to the fit are shown in insert at the top. (*C*) Structure comparison of TraC with close homologs. (*Left*) Structural superposition of TraC (yellow ribbon) with the 11S regulator of the 20S proteasome (red ribbon). (*Right*) Structural superposition of TraC (yellow ribbon) with the focal adhesion targeting region of the focal adhesion kinase (purple). (*D*) Accumulation and cellular fractionation of the *TraC*/*TraC mutant* gene products in *E. coli*. (*Da*) TraC in cell lysates from *E. coli* FM433 pKM101*traC*1134::Tn5 carrying pTrcTraC wild type or its mutant variants. (*Db*) TraC in extracellular high molecular mass fractions isolated from *E. coli* FM433 pKM101*traC*1134::Tn5 carrying pTrcTraC or its mutant variants. Lanes were loaded with 10 μl of an SDS lysate of cells grown to identical optical density. TraC and TraC variants were detected by anti-TraC antibody after Western blotting.

genta). Three patches of hydrophobic conserved residues stand out (in deep blue in Fig. 1*D*): one located on top of the appendage (residues L86 and P87), another located on the same side of the protein but at the base of the major three helix bundle on the N-terminal apical side of the molecule (residue I176), and finally a third also located in the same region but on the other side of the molecule (residue L163, I167, and L179). TraC contains a large amount of Gln residues and some of them are strictly conserved among VirB5 proteins. Notably, a cluster is clearly visible on one side of the protein (in green in Fig. 1*D Left*) in the three-helix bundle region. High degree of conservation may have functional significance. This prompted us to mutate some of the conserved residues and assess the function of the resulting protein variants in several biological assays (see below).

Assembly State of TraC. TraC has been described as a dimer in solution based on size exclusion chromatography results (23). TraC, in the crystal, is involved in five different intermolecular crystal packing interfaces. One of them stands out with a buried surface area of 1,720 Å^2, compared with ≈700 Å^2 for the four others (shown in Fig. 2*A*). Protein–protein interactions in this interface are formed by residues in the 136–151 region of the sequence that encompasses residues at the end of helix αd, in the loop between αd and α2, and residues at the top end of helix α2. These residues contact their symmetry equivalent across the interface. If dimerization is important for the function of TraC, then disrupting the only credible protein–protein interface observed in the crystal should result in disruption of protein function. Thus, we generated TraC variants mutated in three residues located in this interface, Thr-69 (T69I, T69E, T69W), Asp-142 (D142R, D142E), and Val-144 (V144W, V144E, V144I, V144D). All mutants were checked for aggregation by using dynamic light scattering and for proper folding by using circular dichroism.

We first analyzed the oligomeric state of TraC and TraC mutants by using biochemical techniques. Size exclusion chromatography of purified TraC (either 2 or 12 mg/ml) confirmed that the protein elutes at a volume corresponding to one and a half the predicted molecular mass of TraC. Surprisingly, all TraC mutants examined had molecular masses similar to that of wild-type TraC (data not shown). These results indicate that the major interface in the crystal structure is not used for TraC dimerization. However, one other possible interpretation led us to question whether TraC is indeed a dimer in solution. The fact that TraC elutes at a molecular weight above its predicted one may be due to the fact that TraC is an elongated molecule, not to dimerization.

This prompted us to examine the oligomeric state of TraC by using sedimentation equilibrium methods (Fig. 2*B*). All data could be globally fit to a single species (root mean square fit of 0.0045). Nonideality was not observed, and the residuals revealed no systematic deviations (Fig. 2*B*). The NONLIN program produced a σ value of 0.9736, corresponding to a calculated molecular mass for TraC of 19,785 Da (19,659–19,911 Da), which is within 9.3% of the expected molecular weight of the monomeric TraC (23,496 Da). Additionally, two TraC variants mutated in the putative dimerization interface (T69I and

Table 2. Complementation of the *traC* insertion derivative of pKM101

TraC	Cell-bound TraC*	Exo HMW TraC*	Conj. transf., %	IKe, %	PRD1, %
Wild-type	+++	+++	100	100	100
T69W	+++	+	0.002	ND	ND
T69E	+++	+	0.001	<0.001	<0.001
T69I	+++	+	0.002	ND	ND
D142E	+++	+++	0.7	<0.001	<0.01
D142R	+/−	−	0.002	<0.001	<0.01
V144E	+++	+++	60	70	0.5
V144W	+++	+++	10700	75	4
V144D	+++	+++	76	76	3
V144I	+++	+++	90	94	100
L163A	+++†	+†	0.3	<0.001	<0.01
I167A	+++†	+†	0.001	<0.001	<0.01
Q180A	+++	+++	122	92	45
Q191A	+++	+++	78	90	80

Results of conjugative transfer (Conj. transf.) and phage infections (IKe and PRD1) are reported as average of four to five independent experiments. Exo HMW TraC reports TraC in exocellular high-molecular weight fractions. ND, not determined.

*Amounts were assessed by quantitation of the results from three independent experiments.

†Apparently higher molecular mass after SDS/PAGE.

D142R) also yielded σ values similar to wild-type TraC. We therefore conclude that TraC is a monomer in solution.

Stability of TraC Variants in *E. coli* and Pilus Incorporation. We next examined the TraC variants described above (Thr-69, Asp-142, and Val-144) and other mutants altered in some of the conserved surface regions of TraC, L163A, I167A, Q180A, and Q191A (Fig. 1*D*) for their stability and their incorporation into the pilus (Fig. 2*D*). Only very small amounts of the D142R variant of TraC were detected in cell lysates, indicating that the stability of this protein was strongly reduced (although it is stable when overproduced in *E. coli*, and subsequently purified, see above). As a result, this variant is not detected in the pilus fraction. L163A and L167A ran as slightly higher molecular masses species (denoted as an asterisk in Fig. 2*D*), were detected in the cells at wild-type level, and were not efficiently incorporated in the pilus. Cellular levels for all T69 variants were as wild type; however, their incorporation into the pili was considerably reduced (Fig. 2*D*). These mutations did not affect the stability of TraC in the cell, but the incorporation into the extracellular pilus structure was clearly reduced. Wild-type levels of detection both in the cells and the pili were observed for all other TraC variants.

Complementation of Conjugative Transfer and Phage Receptor Functions. We next assessed the role of TraC and TraC variants in pilus assembly and function. Formation of pili is required for conjugative plasmid transfer. Moreover, pili are essential attachment devices for bacteriophages. Thus, we examined the effect of TraC and the TraC variants in these two processes, conjugative plasmid transfer and phage attachment and infection.

Conjugative plasmid transfer was monitored as described in (23). Results are reported in Table 2. In all mutants except for the D142E and V144W variants, the ability to mediate conjugative transfer is strongly correlated with localization in the pilus. All T69 variants and the D142R, L163A and I167A variants, which are unable to incorporate into high-molecular mass structures, are also unable to support conjugative transfer. Conversely, V144E, V144D, V144I, Q180A, and Q191A, which readily incorporate into pili, are also able to mediate conjugative transfer (Table 2). These results show that incorporation of TraC into pili is a prerequisite for conjugative plasmid transfer.

Two mutants exhibited unusual properties. The D142E variant is greatly affected in its ability to mediate conjugative transfer despite the fact that its amount level in the pilus fraction is comparable to wild type. Remarkably, the V144W derivative displays dramatically increased levels of conjugative plasmid transfer and its level in the pilus fraction is similar to wild type (Table 2).

Because of the low abundance of IncN pili in the natural system, electron microscopy cannot be used for the quantification of pilus formation. However, binding of phages IKe or PRD1 and subsequent infection depends on the presence of pili (34–36). Thus, the infection of IncN pilus-producing *E. coli* by these bacteriophages can be exploited as an assay for pilus assembly.

pTrcTraC-carrying cells produced relatively high levels of TraC. Because the high levels of TraC interfered with both IKe and PRD1 phage infection (not shown), the *traC* wild type and the mutated genes were cloned into pVSBAD, which allows the production of lower protein levels. *E. coli* FM433 pKM101*traC* carrying pVSBADTraC wild type and the mutated derivatives were first tested in conjugation assays. Qualitatively identical results as those reported above were obtained (not shown). Next, the cells were mixed with different dilutions of phages IKe or PRD1 followed by the quantification of plaque formation in soft agar containing TraC-producing cells. The results of the IKe infection experiments largely paralleled those of the conjugation assays, showing that conjugative transfer ability correlates with the formation of IKe binding sites on the extracellular pili (Table 2). The results with phage PRD1 were similar with the surprising exception of three V144 derivatives. Whereas V144I-producing cells were infected with equal efficiency by PRD1 and IKe, the efficiency of PRD1 infection was very much reduced in V144D, V144E, and V144W-producing cells. These results suggest a role for TraC in the process mediating recognition and attachment of bacteriophages.

Discussion

The fold of TraC/VirB5 is a three-helix bundle decorated by a globular appendage. Search for structural homologs using the program DALI (37) returned very high score hits for a number of proteins that have divergent function. Eight structures returned a Z score of ≥ 5, with two of them, the 11S regulator of the 20S proteasome (38) and the focal adhesion targeting region of the focal adhesion kinase (39), scoring a value >6 (Fig. 2*C*). Thus, by itself, the fold does not provide clues as to the role that TraC/VirB5 proteins may play in conjugation, phage recognition, or type IV secretion. Much more informative is the nature of the protein surface. Notably, we identified a region of the protein surface that is involved in a very large crystal packing interface and that, when mutated, considerably affects TraC function. Indeed, of all mutants examined, the most notable phenotypes were observed for those mutants that affect residues located in that region.

A detailed study of crystal packing interfaces has revealed that surfaces implicated in large interfaces ($<1{,}500$ Å^2) are likely to be involved in protein–protein interaction (40). Moreover, we identified two variants in the large crystal packing interface, D142E and V144W, that have the remarkable properties of being incorporated in the pilus, and yet they affect conjugative transfer dramatically by either decreasing it (D142E) or increasing it (V144W). The D142E variant is also defective in supporting both PRD1 and IKe phage infection, whereas the V144W mutant is defective in promoting infection by PRD1, although infection by IKe proceeds successfully. Thus, we generated TraC proteins able to locate to the pilus, but unable to carry out either all pilus functions (D142E) or selective ones (V144W). Taken

MICROBIOLOGY

altogether, we would like to propose that TraC/VirB5 is involved in protein–protein interactions that promote pilus-mediated functions, and that the large packing interface that we have observed is the region of interaction.

One possible interpretation of the results presented here is that VirB5 proteins are involved in protein–protein interactions, which mediate two particular pilus functions, bacterial attachment leading to conjugative transfer and phage attachment. Bacterial attachment is a key event not only in the early stages of most infectious diseases, but also more generally in processes requiring interaction of the bacteria either with a living cell, a phage, or with any surface (41). Recognition and attachment are mediated by adhesins on the surface of the microbe interacting with receptors displayed on the surface of the cell or phage (41). Could VirB5 proteins be involved directly in the adhesion process? In the absence of direct evidence, it is indeed very speculative to suggest such a role. Intriguingly, the *B. pertussis* Ptl does not contain a VirB5 homolog. This is consistent with the fact that the *B. pertussis* Ptl T4SS is used to secrete the pertussis toxin effector and thus may not require cell–cell contacts and pilus formation, thus making a VirB5 adhesin likely redundant (42).

VirB5 proteins appear to locate in various compartments of the cell. It is found in the membrane, periplasm, and pilus. The pilus may be an end point for VirB5 assembly into the T4SS, and thus, locations other than the pilus (membrane and periplasm) may constitute transit points for VirB5 proteins before their final incorporation into the pilus. Our results may provide additional information about the location of VirB5 on the pilus. Indeed, we found three TraC variants (V144E, V144W, and V144D) that were able to discriminate between two bacteriophages, IKe and PRD1. Although wild-type TraC renders the cells susceptible to infection by both phages, the V144E, V144W, and V144D TraC variants mediates infection of IKe only. IKe is a filamentous single-stranded DNA phage that has been shown to attach to the tip of the pili (35). In contrast, PRD1 is an icosahedral double-stranded DNA phage, which is usually detected at the outer membrane of plasmid-carrying cells, indicating that it may bind at the base of the pilus (35). How the TraC variants could discriminate between the two phages is unclear. However, it could be that TraC decorates the pilus in various places, notably the end and the base, and thus can be involved in the process of phage attachment at both locations. Then TraC variants could selectively be affected in one or other phage infection processes. It is important to note that our study does not provide any evidence that the high molecular weight structures isolated from TraC mutant strains morphologically resemble those from wild-type cells. Thus, a possible interpretation of our results could be that some of the mutant TraC proteins, although able to incorporate into the pilus, may affect pilus biogenesis and produce shorter pili. Other interpretations include the possibility that some mutants may disrupt formation or activity of the secretion channel.

The structure of TraC provides the first structural model for VirB5 proteins and, thus, is an important milestone in the elucidation of the mechanism of type IV secretion. The identification of mutants of TraC/VirB5 where conjugative transfer and pilus biogenesis are uncoupled demonstrates that VirB5 proteins are valid targets for the design of novel antibiotic compounds. In this respect, the structure of TraC provides a unique template that can be used for structure-based drug design.

We thank the staff of beamline 19BM of the Structural Biology Center at APS (Argonne National Laboratory) for help during data collection. This work was supported by National Institutes of Health Grant AI49950 and Wellcome Trust Grant 065932 (to G.W.), National Sciences and Engineering Council of Canada Grant 262104, and the European Union Frame Program 5 under Contract QLK2-CT-2001-01200 (to C.B.).

1. Ochman, H., Lawrence, J. G. & Groisman, E. A. (2000) *Nature* **405,** 299–304.
2. Baron, C., O'Callaghan, D. & Lanka, E. (2002) *Mol. Microbiol.* **43,** 1359–1366.
3. Christie, P. J. (2001) *Mol. Microbiol.* **40,** 294–305.
4. Zupan, J., Muth, T. R., Draper, O. & Zambryski, P. C. (2000) *Plant J.* **23,** 11–28.
5. Boschiroli, M. L., Ouahrani-Bettache, S., Foulongne, V., Michaux-Charachon, S., G., B., Allardet-Servent, A., Cazevieille, C., Lavigne, J. P., Liautard, J. P., Ramuz, M. & O'Callaghan, D. (2002) *Vet. Microbiol.* **90,** 341–348.
6. Roy, C. R. & Tilney, L. G. (2002) *J. Cell Biol.* **158,** 415–419.
7. Eisenbrandt, R., Kalkum, M., Lai, E. M., Lurz, R., Kado, C. I. & Lanka, E. (1999) *J. Biol. Chem.* **274,** 22548–22555.
8. Lai, E.-M. & Kado, C. I. (1998) *J. Bacteriol.* **180,** 2711–2717.
9. Sagulenko, V., Sagulenko, E., Jakubowski, S., Spudich, E. & Christie, P. J. (2001) *J. Bacteriol.* **183,** 3642–3651.
10. Schmidt-Eisenlohr, H., Domke, N., Angerer, C., Wanner, G., Zambryski, P. C. & Baron, C. (1999) *J. Bacteriol.* **181,** 7485–7492.
11. Beaupré, C. E., Bohne, J., Dale, E. M. & Binns, A. N. (1997) *J. Bacteriol.* **179,** 78–89.
12. Das, A. & Xie, Y.-H. (2000) *J. Bacteriol.* **182,** 758–763.
13. Kumar, R. B. & Das, A. (2001) *J. Bacteriol.* **183,** 3636–3641.
14. Fernandez, D., Spudich, G. M., Zhou, X.-R. & Christie, P. J. (1996) *J. Bacteriol.* **178,** 3168–3176.
15. Dang, T. A., Zhou, X.-R., Graf, B. & Christie, P. J. (1999) *Mol. Microbiol.* **32,** 1239–1253.
16. Krause, S., Barcena, M., Pansegrau, W., Lurz, R., Carazo, J. M. & Lanka, E. (2000) *Proc. Natl. Acad. Sci. USA* **97,** 3067–3072.
17. Kumar, R. B. & Das, A. (2002) *Mol. Microbiol.* **43,** 1523–1532.
18. Sagulenko, E., Sagulenko, V., Chen, J. & Christie, P. J. (2001) *J. Bacteriol.* **183,** 5813–5825.
19. Yeo, H.-J., Savvides, S. N., Herr, A. B., Lanka, E. & Waksman, G. (2000) *Mol. Cell* **6,** 1461–1472.
20. Savvides, N. S., Yeo, H.-J., Beck, M. R., Blaesing, F., Lurz, R., Lanka, E., Buhrdorf, R., Fisher, W., Hass, R. & Waksman, G. (2003) *EMBO J.* **22,** 1969–1980.
21. Gomis-Ruth, F. X., Moncalian, G., Perez-Luque, R., Gonzalez, A., Cabezon, E., de la Cruz, F. & Coll, M. (2001) *Nature* **409,** 637–641.
22. Llosa, M., Gomis-Ruth, F. X., Coll, M. & de la Cruz, F. (2002) *Mol. Microbiol.* **45,** 1–8.
23. Schmidt-Eisenlohr, H., Domke, N. & Baron, C. (1999) *J. Bacteriol.* **181,** 5563–5571.
24. Krall, L., Wiedemann, U., Unsin, G., Weiss, S., Domke, N. & Baron, C. (2002) *Proc. Natl. Acad. Sci. USA* **99,** 11405–11410.
25. Otwinowski, O. & Minor, W. (1997) *Methods Enzymol.* **276,** 307–326.
26. Terwilliger, T. C. & Berendzen, J. (1999) *Acta Crystallogr. D* **55,** 849–861.
27. Brünger, A. T., Adams, P. D., Clore, G. M., DeLano, W. L., Gros, P., Grosse-Kunstleve, R. W., Jiang, J. S., Kuszewski, J., Nilges, M., Pannu, N. S., *et al.* (1998) *Acta Crystallogr. D* **54,** 905–921.
28. Jones, T. A. & Thirup, S. (1986) *EMBO J.* **5,** 819–822.
29. Jones, T. A., Zou, J. Y., Cowan, S. W. & Kjeldgaard, M. (1991) *Acta Crystallogr. A* **47,** 110–119.
30. Cellini, C., Kalogeraki, V. S. & Winans, S. C. (1997) *Plasmid* **37,** 181–188.
31. Laue, T. M., Shah, B. D., Ridgeway, T. M. & Pelletier, S. L. (1992) *Computer-Aided Interpretation of Analytical Sedimentation Data for Proteins* (Royal Society of Chemistry, London).
32. Johnson, M. S. & Doolittle, R. F. (1986) *J. Mol. Evol.* **23,** 267–278.
33. Bowie, J. U., Lüthy, R. & Eisenberg, D. (1991) *Science* **253,** 164–170.
34. Bradley, D. E. (1979) *Plasmid* **2,** 632–636.
35. Frost, L. S. (1993) in *Bacterial Conjugation*, ed. Clewell, D. B. (Plenum, New York), pp. 189–221.
36. Olsen, R. H., Siak, J.-S. & Gray, R. H. (1974) *J. Virol.* **14,** 689–699.
37. Holm, L. & Sander, C. (1998) *Nucleic Acids Res.* **26,** 316–319.
38. Knowlton, J. R., Johnston, S. C., Whitby, F. G., Realini, C., Zhang, Z., Rechsteiner, M. & Hill, C. P. (1997) *Nature* **390,** 639–643.
39. Arold, S. T., Hoellerer, M. K. & Noble, M. E. (2002) *Structure (London)* **10,** 319–327.
40. Janin, J. & Rodier, F. (1995) *Proteins* **23,** 580–587.
41. Soto, G. E. & Hultgren, S. J. (1999) *J. Bacteriol.* **181,** 1059–1071.
42. Burns, D. L. (2003) *Curr. Opin. Microbiol.* **6,** 29–34.
43. Carson, M. (1997) *Methods Enzymol.* **277,** 493–505.